2026 IEEE International Conference on Robotics and Automation (ICRA 2026)
June 1-5, 2026. Vienna, Austria

Programmable Assembly and Cooperative Manipulation of Heterogeneous Microspheres via Optoelectronic Tweezers

Wenyan Niu[1], Ao Wang[1], Shunxiao Huang[1], Jingwen Ye[1], Zaiyang Chen[1], Chan Li[1], Hongyan Sun[1], Zijin Zeng[1], Yingjian Guo[1*], and Lin Feng[1,2*]

***Abstract*— The programmable assembly and actuation of micro- and nanostructures remain key challenges in the development of micro-robotics. This work presents a programmable assembly and cooperative actuation strategy for heterogeneous microspheres based on optoelectronic tweezers (OET). By employing Ag-PS microspheres as actuators and PS microspheres as payloads, we constructed stable "actuator–payload" units and investigated their frequency response and dynamic characteristics. The proposed method enables controlled assembly into core–satellite and satellite–core configurations with tunable coordination angles. Furthermore, the cooperative effect of the dual actuating units was revealed, enabling the composite system to maintain a continuous and precise circular trajectory following a ring-shaped light pattern. In addition, the modular assembly strategy was used to construct chain-like structures exceeding 172 μm in length, thereby confirming the approach's scalability. This work expands the application of OET from particle transport to modular microstructure construction and multi-actuator cooperative control, offering new opportunities for designing microbotic systems and their biomedical applications.**

I. Introduction

Microrobots hold great promise for applications in drug delivery, cell recognition, and biomedicine, where their functional performance relies on the precise manipulation and programmable assembly of micro/nanoparticles[1]. Optoelectronic tweezers (OET), as a non-contact micromanipulation technique, replace traditional metallic electrodes with optically defined virtual electrodes[2]. Compared with optical tweezers[3], magnetic tweezers[4], and acoustic tweezers[5], OET enables high-throughput and high-precision operations under low light intensity, significantly reducing photothermal damage[6]. These advantages have made OET widely applied in particle manipulation[7], cell screening[8], and microstructure fabrication[9].

Currently, OET has been demonstrated to rapidly concentrate and separate homogeneous microparticles via dielectrophoresis (DEP) forces and AC electroosmosis (ACEO) flow[10, 11]. Moreover, particles with different dielectric properties, such as metallic microspheres and polystyrene microspheres, have been exploited to drive collective motion[12, 13]. However, most of these studies have focused on transport functionality, without exploring the potential of constructing and actuating stable functionalized microstructures. A critical challenge thus remains: to move beyond simple transport tasks toward programmable, stable, and scalable strategies for microstructure construction.

To address this challenge, we propose a novel OET-based strategy for heterogeneous microsphere functional assembly and cooperative actuation. Specifically, Silver-coated polystyrene (Ag-PS) microspheres are employed as actuating units, while polystyrene (PS) microspheres serve as passive loads, forming a fundamental "actuator-payload" unit. We systematically investigate its frequency-dependent response and dynamic behaviors. By tuning the electric field frequency and optical field parameters, the coordination number of assembled structures can be dynamically controlled, enabling highly programmable directional assembly. Furthermore, we demonstrate a cooperative driving effect: two Ag-PS microspheres collaboratively towing a PS microsphere achieve stable circular motion along a ring-shaped optical pattern, exhibiting superior motion stability and trajectory tracking capability. Finally, by employing a hierarchical assembly strategy, we successfully constructed chain-like structures up to 172 μm in length, confirming both the scalability and robustness of the approach. Overall, this work extends the application of OET from particle transport to microstructure construction and cooperative actuation, providing a new framework for modular design and scalable fabrication of microrobotic systems with potential applications in targeted drug delivery and biomedical micromanipulation.

II. Materials and Method

A. Sample Preparation

PS microspheres (polystyrene, diameter: 30 μm, aqueous suspension, MicroNano Intelligent Technology Co., Ltd.) were used as passive payload particles. Silver-coated polystyrene microspheres (Ag-PS, diameter: 15 μm) were fabricated via an electroless plating process, yielding a conformal silver shell with a thickness of approximately 80-100 nm.

For sample preparation, 3 μL of PS microsphere suspension and an appropriate amount of Ag-PS microspheres were dispersed in 10 mL of deionized water to obtain a homogeneous working suspension. Subsequently, a 10 μL aliquot of this suspension was injected into the chamber of the OET chip for manipulation experiments. The suspending

This work was supported by the Beijing Municipal Fund for Distinguished Young Scholars (Grant No. JQ22022) and the National Key RD Program of China (Grant No. 2022YFF1502000).

[1]Wenyan Niu, Ao Wang, Shunxiao Huang, Jingwen Ye, Zaiyang Chen, Chan Li, Hongyan Sun, Zijin Zeng, Yingjian Guo, and Lin Feng are with Beihang University, School of Mechanical Engineering and Automation, Beijing, 100083, China (e-mail: by2407157@buaa.edu.cn)

[2]Lin Feng is also with the Beihang University, Beijing Advanced Innovation Center for Biomedical Engineering, and the School of Mechanical Engineering and Automation, Beijing 100083, China.

*Correspondence: yingjguo@126.com Yingjian Guo
linfeng@buaa.edu.cn Lin Feng

medium was an aqueous solution with a conductivity of 2×10^{-3} S/m and a relative permittivity of 80. The PS microspheres had a conductivity of 2×10^{-4} S/m and a relative permittivity of 2.58, while the Ag-PS microspheres exhibited a conductivity of 6.3×10^{6} S/m and a relative permittivity of 10^{7}[14].

B. Experimental Platform

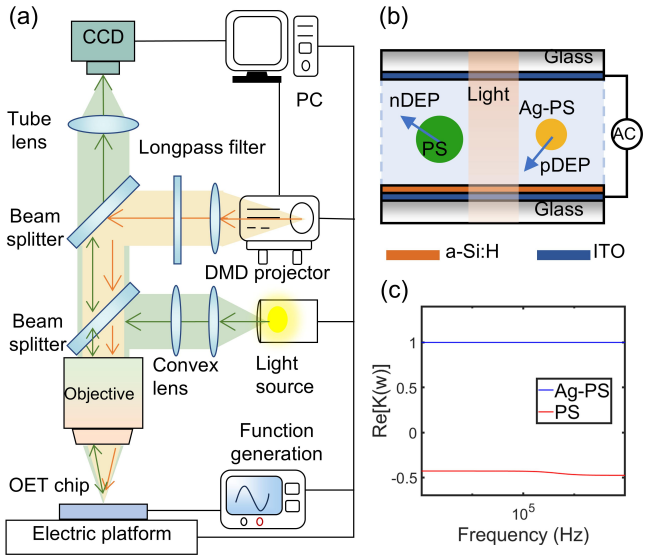

Figure 1. Schematic of the system and CM factor calculation results. (a) Schematic of the optical system. (b) Schematic of the OET chip. (c) The real part of the CM factor for PS and Ag-PS microspheres at different frequencies.

The operational light (610nm) is generated by a digital micromirror device (DMD) projector (DLP6500, Texas Instruments) under computer control, and projected onto the OET chip to create spatially programmable electric field distributions. By modulating the local photoconductivity of the a-Si:H layer, the projected optical patterns dynamically define virtual electrodes for particle manipulation. The optical observation system comprises a 5× objective lens (UPLFLN4X, Olympus), a tube lens (SWTLU-C), and a 4K CCD camera (U3120-23C, LBAS), enabling real-time tracking of microsphere motion. The illumination uniformity and image clarity are optimized by fine adjustment of a convex lens. The electrical driving signal is provided by a function generator (DG1022Z, RIGOL), which applies an alternating electric (AC) field across the top and bottom ITO electrodes of the chip. The chip is mounted on a motorized XYZ translation stage for precise positioning and automated focus adjustment (Fig. 1a).

The OET chip consists of two ITO-coated glass substrates, with the bottom substrate coated with a hydrogenated amorphous silicon (a-Si:H) photoconductive layer via plasma-enhanced chemical vapor deposition (PECVD), and the interspace serving as the liquid chamber for particle suspension (Fig. 1b).

C. Interaction simulation

In OET, neutral particles acquire motility through dielectric polarization, with their motion primarily governed by the DEP force. The characteristics of the DEP force are determined by the real part of the Clausius–Mossotti factor ($\mathrm{Re}[K(\omega)]$), which reflects the polarization characteristics of the particle relative to the surrounding medium. The Clausius–Mossotti factor is calculated as follows[15]:

$$K(\omega)=\frac{\varepsilon_p^*-\varepsilon_m^*}{\varepsilon_p^*+2\varepsilon_m^*},\ \varepsilon_m^*=\varepsilon_m-j\frac{\sigma_m}{\omega},\ \varepsilon_p^*=\varepsilon_p-j\frac{\sigma_p}{\omega} \quad (1)$$

where ε_p and ε_m represent the permittivity of the particle and the medium, respectively; σ_p and σ_m are the conductivity of the particle and the medium; and ω is the angular frequency.

According to the value of $\mathrm{Re}[K(\omega)]$, DEP force can be divided into positive DEP (pDEP) force and negative DEP (nDEP) force. When $\mathrm{Re}[K(\omega)]$ is greater than 0, the particles are more easily polarized than the medium and are easily attracted to the illumination area of a strong electric field. When $\mathrm{Re}[K(\omega)]$ is less than 0, the object is subject to repulsion and is more likely to enter the dark region of the weak electric field[15]. The real part of the Clausius – Mossotti factor as a function of frequency was calculated for both types of microspheres (Fig. 1c). The results indicate that, across the investigated frequency range, Ag-PS microspheres consistently undergo pDEP force, which facilitates their effective attraction to the light spot. In contrast, PS microspheres experience nDEP force, allowing their trajectories to be flexibly controlled by the donut-shaped light pattern.

The DEP force on spherical particles in a non-uniform electric field can be roughly calculated by the following formula[16]:

$$\vec{F}_{DEP}=2\pi r^3\varepsilon_{\mathrm{m}}\,\mathrm{Re}[K(\omega)]\nabla\vec{E}^2 \quad (2)$$

where r represents the radius of the particle and $\nabla\vec{E}^2$ represents the gradient of the electric field's square. More precise force calculations are carried out by the Maxwell stress tensor method:

$$\vec{F}_{DEP}=\int T^{MST}\cdot\vec{n}\mathrm{d}S \quad (3)$$

where S represents the surface enclosing the particle, $\vec{n}$ represents the unit vector perpendicular to dS , and represents the Maxwell stress tensor. By simulating the forces acting on microspheres, the interaction forces between particles can be quantitatively analyzed.

In OET, polarized particles in proximity interact with each other, and particles with distinct dielectric properties exhibit attractive forces[17]. To investigate the interaction mechanism of heterogeneous particles, numerical simulations were performed using COMSOL Multiphysics 6.2 (COMSOL Inc., Stockholm, Sweden). The model geometry was set with a liquid chamber height of 80 μm, a light spot diameter of 20 μm, PS microspheres of 30 μm, and Ag-PS microspheres of 15 μm. Electrical parameters were configured as 10 Vpp at 100 kHz, with the amorphous silicon thin film having a photoconductivity of 1×10^{-3} S/m and a dark conductivity of 1×10^{-11} S/m.

Fig. 2 demonstrates the interaction between PS and Ag-PS microspheres in the OET system. In Fig. 2a, the simulated

velocity field distribution is presented. The color map represents the magnitude of the fluid velocity, while the black streamlines indicate the circulation pattern induced by the optically modulated electric field. The red arrows denote the local velocity vectors in the vicinity of the particles. The simulation reveals the formation of asymmetric flow vortices around the illuminated region, resulting in net hydrodynamic coupling between the heterogeneous particles. Fig. 2b shows time-lapse experimental images of the interaction process. The PS and Ag-PS microspheres gradually approach each other, consistent with the simulated flow-induced transport behavior. The observed motion results from the combined action of DEP force and light-induced AC electroosmotic (LACE) flow.

The qualitative consistency between simulation and experiment supports the existence of a coupled electrohydrodynamic interaction mechanism, which provides the physical basis for subsequent programmable assembly. In this framework, Ag-PS microspheres function as active driving units (actuators), whereas PS microspheres act as passive loads (payloads).

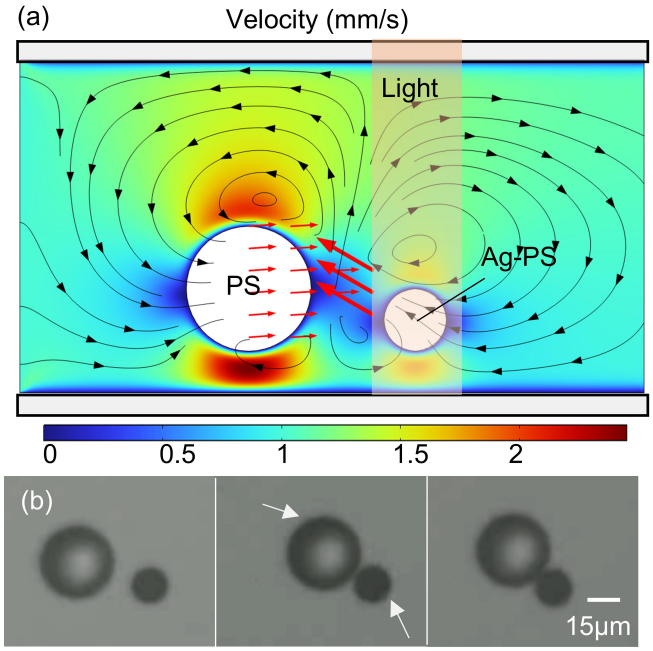

Figure 2. Interaction between PS and Ag-PS microspheres. (a) Velocity field distribution during the interaction of two particles, with red arrows denoting velocity vectors. (b) Experimental image showing the interaction of the two particles within the OET system. White arrows indicate particle displacement direction.

III. Experiment and Results

A. Characterization of Driving Units and Frequency Optimization

The frequency of the applied AC signal plays a pivotal role in OET manipulation, as it directly governs the efficiency of particle assembly and dynamic control[18]. When particles exhibit the same DEP force, they will mutually repulse along the direction of the field[19]. In contrast, when they display opposite DEP responses, this leads to mutual attraction in the perpendicular direction[20]. The simulation results reveal a strong frequency-dependent interaction between PS and Ag-PS microspheres in the OET field. At a low frequency of 10 kHz (Fig. 3a), the electric field is primarily confined around the illuminated Ag-PS microsphere, while the PS microsphere experiences negligible field enhancement, leading to a repulsive interaction as indicated by the opposite Maxwell stress directions on their surfaces. In contrast, at a higher frequency of 300 kHz (Fig. 3b), the electric field distribution becomes more pronounced around the PS microsphere, and the Maxwell stress vectors on both particles point toward each other, indicating a clear attractive interaction. Based on these findings, we selected an AC frequency of 300 kHz for subsequent particle assembly experiments.

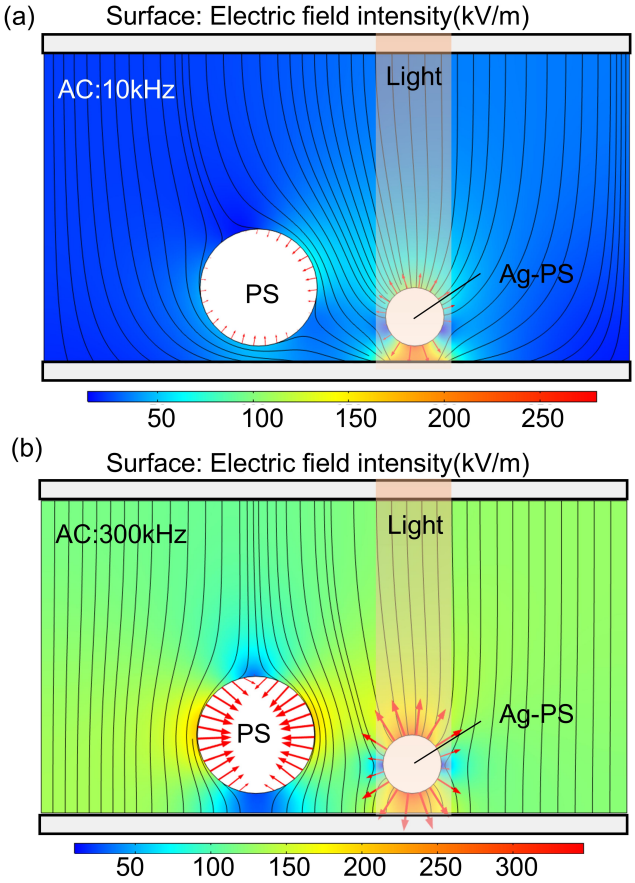

Figure 3. Simulation analysis of particle interactions at different frequencies. (a) Electric field intensity distribution at an AC frequency of 10 kHz. (b) Electric field intensity distribution at 300 kHz. Red arrows indicate the Maxwell stress tensor on the particle surfaces, and black streamlines represent the electric field direction.

To elucidate the dynamic response of composite microspheres in the OET field, we first examined the equilibrium behavior of a basic composite unit consisting of one Ag–PS microsphere coupled with one PS microsphere under different applied frequencies. Experimental results indicate that as the applied frequency decreases from 50 kHz to 30 kHz, the equilibrium position of the composite unit relative to the light spot shifts significantly (Fig. 4a and 4b). Previous studies have demonstrated that for PS microspheres, the light spot exerts a repulsive force via nDEP. At the same time, ACEO flows attract the particles toward the periphery of the light pattern, resulting in a frequency-dependent equilibrium position[21].

Given the microsphere parameters used in this experiment, the PS microsphere has twice the diameter of the Ag-PS microsphere, leading to a significantly stronger nDEP force acting on the PS microsphere compared to the pDEP force on the Ag-PS microsphere. Consequently, we infer that the behavior of the PS microsphere predominantly governs the equilibrium position of the composite unit.

Further analysis of the velocity–frequency curve (Fig. 4c) reveals that the maximum moving velocity of the composite unit initially increases and subsequently decreases with increasing frequency, peaking at 100 kHz. The experimentally measured peak velocity is approximately 45 μm/s. These results demonstrate that the composite unit exhibits pronounced frequency-dependent behavior. Based on this characteristic, a driving frequency of 100 kHz was selected for subsequent multi-particle manipulation experiments to ensure stable and efficient motion of the composite unit.

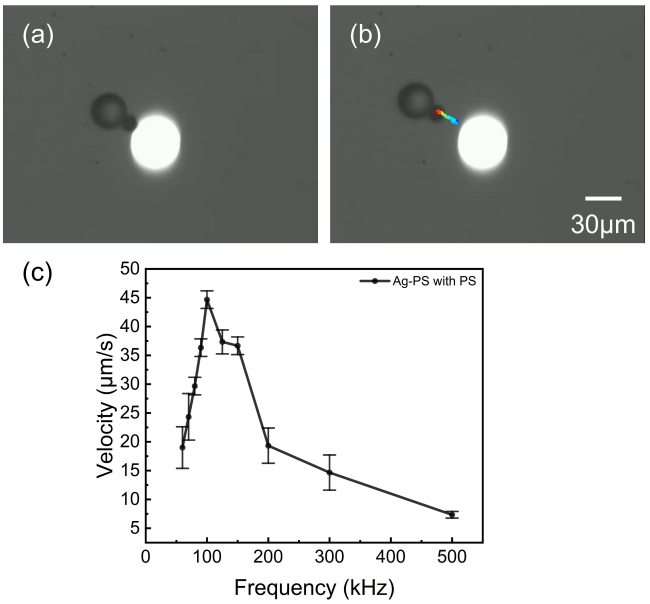

Figure 4. Dynamic response of the composite structural unit at different frequencies. (a) Position of the composite structure at an electric field frequency of 50 kHz. (b) Position of the composite structure at 30 kHz, with colored lines indicating the motion trajectories. (c) Variation of the maximum displacement velocity of the composite unit as a function of electric field frequency.

B. Directed Assembly

Building upon the frequency response characteristics of individual composite units, we further explored the assembly behavior of multi-particle systems. Experimental results show that using Ag-PS microspheres as either cores or satellites enables highly programmable, directed assembly, exhibiting features distinctly different from those of conventional self-assembly.

Core-Satellite Assembly Mode

In the core-centered assembly mode, a single Ag-PS microsphere can sequentially attract multiple PS microspheres, forming a stable core-satellite structure (Fig. 5). In the experiments, we first observed the binding of an Ag-PS microsphere with a single PS microsphere. Additional PS microspheres were then introduced using two strategies: (1) dragging the entire composite unit via the optical spot to bring it closer to the target PS microspheres, and (2) manipulating the target PS microspheres with a donut-shaped optical pattern, gradually bringing them closer to the Ag-PS core. Both approaches exhibited high reproducibility, and the resulting structures remained stable for at least several tens of seconds after removing the light pattern. This indicates sufficiently strong inter-particle interactions to ensure structural stability.

Compared to conventional random aggregation[22], this approach offers advantages of temporal control and structural predictability: the binding sequence and spatial distribution of the particles can be predetermined, avoiding uncontrolled clustering. The core-satellite configuration thus provides a foundation for constructing more complex, multi-connected microstructures.

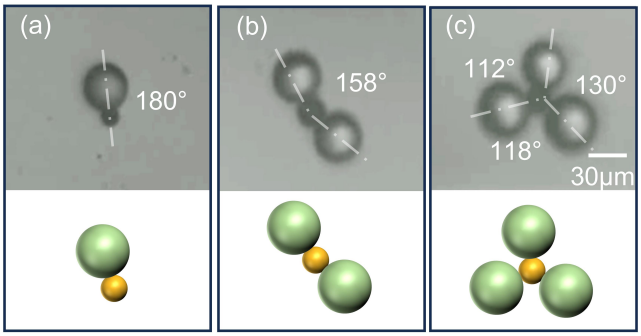

Figure 5. Assembly of a single Ag-PS microsphere with multiple PS microspheres. (a) With one PS microsphere. (b) With two PS microspheres. (c) With three PS microspheres.

Satellite – Core Assembly Mode

In an alternative assembly mode, a single PS microsphere acts as the payload. In contrast, multiple Ag-PS microspheres are guided by optical spots to bind together, forming a satellite-core configuration. This process allows for precise control of the angles between the microspheres. Fig. 6 illustrates the typical angular configurations that occur when two or three Ag-PS microspheres attach to a single PS microsphere. When guiding two Ag-PS microspheres to connect to the core, configurations approaching angles of 120° and 180° can be achieved. For three Ag-PS microspheres, configurations close to 120° and 90° are observed. By adjusting the positions of the optical spots around the core, the angular configurations of the microspheres can be partially predetermined. Importantly, experimental results indicate that these structures remain stable even after the light pattern is removed, which demonstrates that the geometric configurations formed during assembly are effectively "locked in." This not only shows enhanced manipulation precision but also provides a foundation for constructing micro-mechanical structural units with specific functionalities.

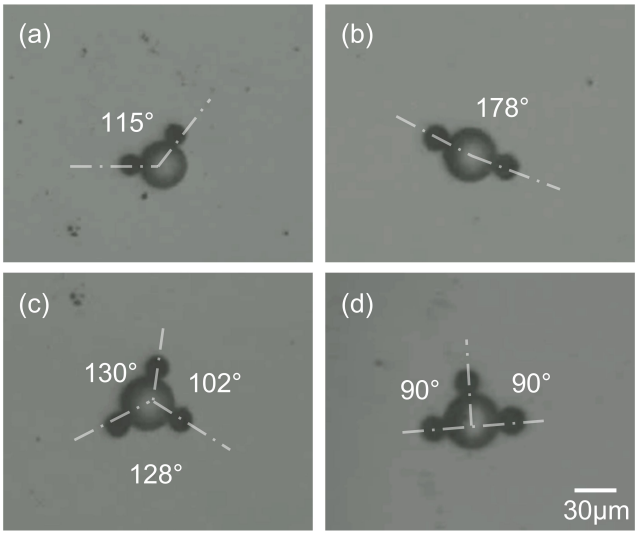

Figure 6. Programmable assembly of satellite-core structures using a single PS microsphere and multiple Ag-PS microspheres. (a, b) Top-view images showing two representative stable configurations formed by two Ag-PS microspheres, demonstrating angular controllability. (c, d) Representative stable configurations achieved with three Ag-PS microspheres.

C. Dynamic Manipulation Capability

Dynamic control performance is a critical evaluation criterion for micro-robotic systems[23]. In our experimental investigation, we observed that when a single Ag-PS microsphere is used to drive a single PS microsphere payload, its ability to move around a large light pattern is significantly constrained. This limitation manifests as a restricted trajectory range and challenges in maintaining stable paths within complex optical fields. In contrast, when two Ag-PS microspheres simultaneously bind to the same PS microsphere, the resulting composite structure demonstrates substantially enhanced motility. Under the actuation of a ring-shaped optical pattern, the system can execute stable, continuous motion along a predefined circular trajectory (Fig. 7).

These results suggest that the cooperative actuation effect provides a scalable approach to overcoming the limitations of single-particle manipulation. Compared to single-particle traction, which is susceptible to displacement or motion interruption due to uneven force distribution, the coordinated action of dual Ag-PS microspheres effectively distributes the driving force across the PS microsphere, resulting in improved controllability and stability within the optical field. This mechanism bears analogy to "dual-arm coordination" in macroscopic robotic systems, where multiple actuators collaborate to accomplish complex motions that are challenging for a single actuator. At the microscale, this cooperative behavior provides a novel strategy for overcoming the limitations of single-particle manipulation.

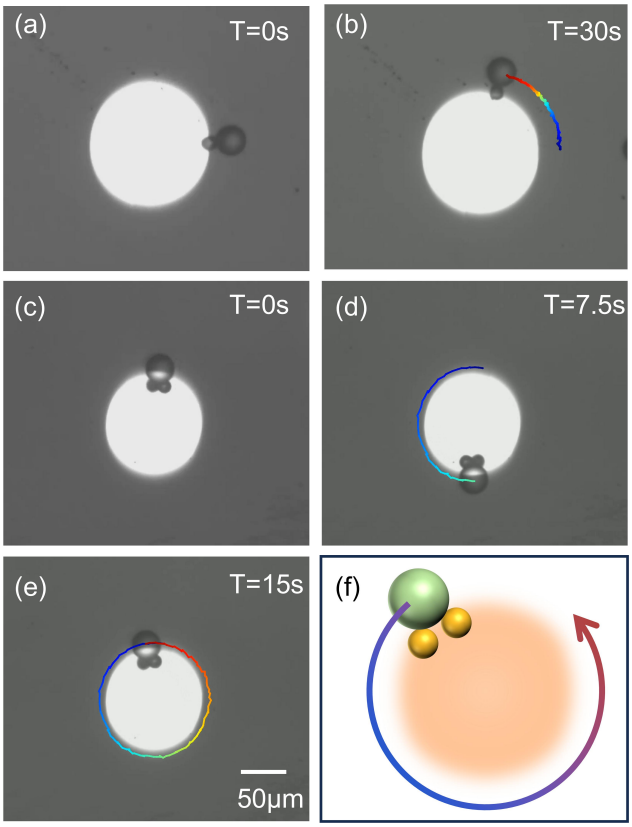

Figure 7. Propulsion of a PS microsphere driven by Ag-PS microspheres. (a)-(b) Experimental snapshots of propulsion driven by a single Ag-PS microsphere. (c)-(e) Time-lapse experimental images showing the propulsion process. Superimposed colored trajectories indicate the displacement paths over time. AC electric field at 100 kHz, 10Vpp. (f) Schematic diagram of the motion of the composite structure.

D. Repeated Assembly of Chain-like Structure

To verify the scalability of our method in constructing macroscopic microstructures, we defined the "one actuator and one payload" binary unit as a standardized module. By systematically repeating the "address-attract-fix" assembly procedure, multiple modules were sequentially connected end-to-end, ultimately forming a chain-like structure with a length exceeding 172 μm within approximately one minute (Fig. 8). Experimental results confirm that this chain-like structure remains stable even after the optical field is removed, indicating that the inter-module interactions are sufficiently robust to maintain integrity. Both the length and stiffness of the chain can be tuned by adjusting the number of assembly steps and particles, thereby providing programmability. This modular and hierarchical assembly strategy overcomes the size limitations of single optical-trap manipulation and enables effective scaling to larger functional microstructures.

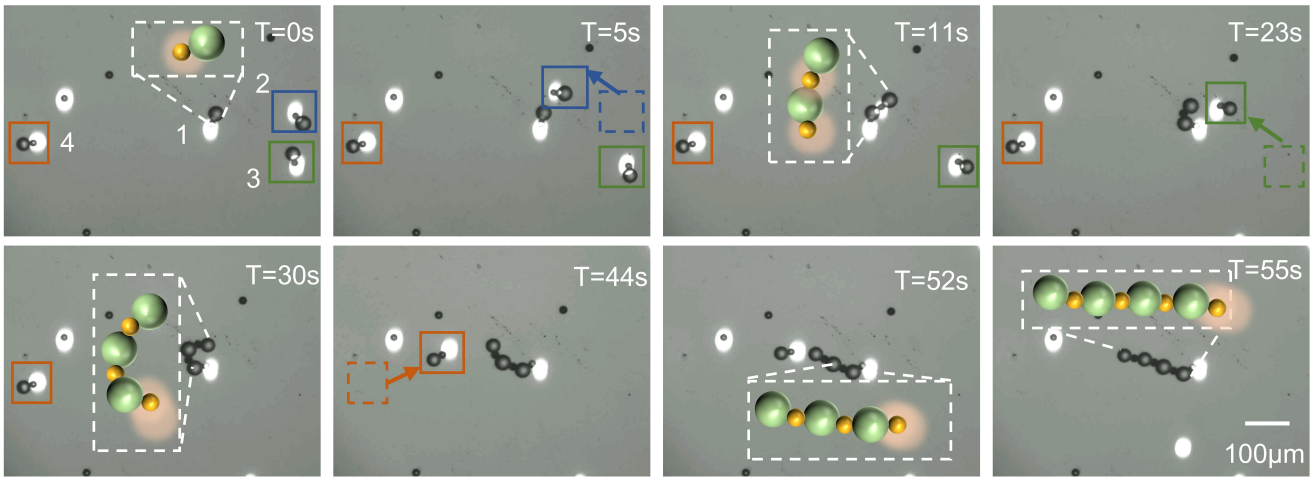

Figure 8. Process of chain-like structure assembly. The orange spheres represent the Ag-PS microspheres, and the green spheres represent the PS microspheres. The Experimental conditions: Actuator-payload unit manipulation: AC electric field at 100 kHz, 10Vpp; Inter-unit assembly: AC electric field at 100 kHz.

IV. Conclusion

In this study, we propose a programmable assembly and cooperative actuation strategy for heterogeneous microspheres based on OET, and investigate the frequency-dependent dynamics of Ag-PS actuator units coupled with PS payloads in non-uniform electric fields. Our results demonstrate that by tuning the electric field frequency and optical parameters, diverse and stable configurations-including core–satellite and satellite-core structures can be precisely assembled, overcoming the randomness of conventional self-aggregation. In terms of locomotion, experiments reveal a cooperative driving effect: dual Ag-PS microspheres significantly enhance motion stability, enabling the composite units to follow continuous, predictable circular trajectories under a ring-shaped optical pattern. Furthermore, we introduce a modular assembly approach, defining the “one Ag-PS and one PS” pair as a functional unit and hierarchically connecting multiple units to construct chain structures exceeding 172 μm in length, thereby validating the method’s scalability. Collectively, this strategy extends the application scope of OET from single-particle manipulation to the assembly of functional microscale architectures and multi-actuator systems. It lays a foundational framework for modular design, cooperative control, and potential biomedical applications such as targeted drug delivery and microscale cargo transport.

References

[1] Y. Tu *et al.*, "Self-propelled supramolecular nanomotors with temperature-responsive speed regulation," *Nature chemistry,* vol. 9, no. 5, pp. 480-486, 2017.

[2] P. Y. Chiou, A. T. Ohta, and M. C. Wu, "Massively parallel manipulation of single cells and microparticles using optical images," *Nature,* vol. 436, no. 7049, pp. 370-2, Jul 21 2005, doi: 10.1038/nature03831.

[3] J. Gieseler *et al.*, "Optical tweezers—from calibration to applications: a tutorial," *Advances in Optics and Photonics,* vol. 13, no. 1, pp. 74-241, 2021.

[4] H. Pan *et al.*, "Morphologically reconfigurable magnetic micropillar arrays using acoustic streaming for particle capture and droplet manipulation," *Sensors and Actuators B: Chemical,* vol. 412, p. 135776, 2024.

[5] Z. Huan *et al.*, "Automated droplet manipulation enabled by a machine-vision-assisted acoustic tweezer," *Sensors and Actuators B: Chemical,* vol. 418, p. 136352, 2024.

[6] S. Zhang *et al.*, "Optoelectronic tweezers: a versatile toolbox for nano-/micro-manipulation," *Chem Soc Rev,* vol. 51, no. 22, pp. 9203-9242, Nov 14 2022, doi: 10.1039/d2cs00359g.

[7] S. Zhang *et al.*, "Manufacturing with light - micro-assembly of opto-electronic microstructures," *Optics Express,* vol. 25, no. 23, 2017, doi: 10.1364/oe.25.028838.

[8] P.-Y. Chu *et al.*, "Utilization of optically induced dielectrophoresis in a microfluidic system for sorting and isolation of cells with varied degree of viability: Demonstration of the sorting and isolation of drug-treated cancer cells with various degrees of anti-cancer drug resistance gene expression," *Sensors and Actuators B: Chemical,* vol. 283, pp. 621-631, 2019, doi: 10.1016/j.snb.2018.12.047.

[9] S. Zhang *et al.*, "Integrated Assembly and Photopreservation of Topographical Micropatterns," *Small,* vol. 17, no. 37, p. e2103702, Sep 2021, doi: 10.1002/small.202103702.

[10] W. Liang, L. Liu, S. H.-S. Lai, Y. Wang, G.-B. Lee, and W. J. Li, "Rapid assembly of gold nanoparticle-based microstructures using optically-induced electrokinetics," *Optical Materials Express,* vol. 4, no. 11, 2014, doi: 10.1364/ome.4.002368.

[11] X. Zhu, Z. Yin, and Z. Ni, "Dynamics simulation of positioning and assembling multi-microparticles utilizing optoelectronic tweezers," *Microfluidics and nanofluidics,* vol. 12, no. 1, pp. 529-544, 2012.

[12] A. Wang *et al.*, "Particle-Assisted Optoelectronic Tweezers for Manipulating Single Cells and Microparticles," *Advanced Science,* p. 2501032, 2025.

[13] S. Liang *et al.*, "Parallel Manipulation and Flexible Assembly of Micro-Spiral via Optoelectronic Tweezers," *Front Bioeng Biotechnol,* vol. 10, p. 868821, 2022, doi: 10.3389/fbioe.2022.868821.

[14] L. Shi *et al.*, "The electrodynamics of rod-like microparticles based on optically induced dielectrophoresis," *Electrophoresis,* vol. 43, no. 21-22, pp. 2175-2183, Nov 2022, doi: 10.1002/elps.202200102.

[15] N. Liu *et al.*, "Automated Parallel Electrical Characterization of Cells Using Optically-Induced Dielectrophoresis," *IEEE Transactions on Automation Science and Engineering,* vol. 17, no. 2, pp. 1084-1092, 2020, doi: 10.1109/tase.2019.2963044.

[16] L. Shi *et al.*, "Continuous separation of microparticles based on optically induced dielectrophoresis," *Microfluidics and Nanofluidics,* vol. 26, no. 1, 2022, doi: 10.1007/s10404-021-02512-0.

[17] S. Liang *et al.*, "Interaction between positive and negative dielectric microparticles/microorganism in optoelectronic tweezers," *Lab Chip,* vol. 21, no. 22, pp. 4379-4389, Nov 9 2021, doi: 10.1039/d1lc00610j.
[18] P. Li *et al.*, "Silver nanostructures synthesis via optically induced electrochemical deposition," *Sci Rep,* vol. 6, p. 28035, Jun 13 2016, doi: 10.1038/srep28035.
[19] H. Hwang and J.-k. Park, "Programmable Cell Manipulation Using Lab-on-a-Display," in *Microfluidics Based Microsystems*, (NATO Science for Peace and Security Series A: Chemistry and Biology, 2010, ch. Chapter 28, pp. 595-613.
[20] Y. Ai, Z. Zeng, and S. Qian, "Direct numerical simulation of AC dielectrophoretic particle–particle interactive motions," *Journal of colloid and interface science,* vol. 417, pp. 72-79, 2014.
[21] J. Zhao *et al.*, "Study of particle equilibrium based on the combination of light-actuated AC electroosmosis and light-actuated dielectrophoresis," *Optics Express,* vol. 32, no. 14, 2024, doi: 10.1364/oe.523241.
[22] H. Yang and Z. Wang, "Effects of light size and intensity on photoconductive effect-based optically-induced dielectrophoresis for three-dimensional manipulation," *Physica Scripta,* vol. 98, no. 5, 2023, doi: 10.1088/1402-4896/acc61a.
[23] S. S. Das and G. Yossifon, "Optoelectronic Trajectory Reconfiguration and Directed Self-Assembly of Self-Propelling Electrically Powered Active Particles," *Adv Sci (Weinh),* p. e2206183, Apr 17 2023, doi: 10.1002/advs.202206183.